Investigation of waste heat recovery system at supercritical conditions with vehicle drive cycles

Article (Accepted Version)

Springer

KSME

Journal of Mechanical Science and Technology 00 (2015) 0000~0000
www.springerlink.com/content/1738-494x

Investigation of waste heat recovery system at supercritical conditions with vehicle drive cycles

Jahedul Islam Chowdhury[1], Bao Kha Nguyen[1,*] and David Thornhill[1]

[1] *School of Mechanical and Aerospace Engineering, Queen's University Belfast, BT9 5AH, United Kingdom*

(Manuscript Received 000 0, 2015; Revised 000 0, 2015; Accepted 000 0, 2015) -please leave blank

Abstract

Waste heat recovery (WHR) for internal combustion engines in vehicles using organic Rankine cycle (ORC) has been a promising technology recently. The operation of the ORC WHR system in supercritical conditions has a potential to generate more power output and thermal efficiency compared with the conventional subcritical conditions. However, in supercritical conditions, the heat transfer process in the evaporator, the key component of the ORC WHR system, becomes unpredictable as the thermo-physical properties of the working fluid changes with the temperature. Furthermore, the transient heat source from the vehicle's exhaust makes the operation of the WHR system difficult. This paper investigates the performance of the ORC WHR system at supercritical conditions with engine's exhaust data from real city and highway drive cycles. The effects of operating variables, such as refrigerant flow rates, evaporator and condenser pressure, and evaporator outlet temperature, on the performance indicators of the WHR system in supercritical conditions are examined. Simulation of operating parameters and the boundary of the WHR system are also included in this paper.

Keywords: Finite volume method; Organic Rankine cycle; Supercritical conditions; Waste heat recovery

1. Introduction

Almost two third of the fuel energy absorbed by an internal combustion engine is wasted via the exhaust and cooling systems [1-3]. The wasted energy makes the engine less economic and is one of the major causes of thermal pollution. To improve the efficiency of the engine, extensive research has been carried out on the waste heat recovery (WHR) system in recent years. The WHR system converts the exhaust or coolant heat into either mechanical rotation or electrical power, which increases the thermal efficiency and, as a result, reduces the fuel consumption of the engine [4, 5]. Two established technologies of WHR can be found in existing literature: the thermoelectric generator (TEG) [6, 7] and the fluid based power cycle [4]. A TEG consists of two dissimilar metals joined together, which converts the heat energy to electrical power. A fluid based power cycle is a combination of several thermodynamic processes and generally involves a working fluid that collects the waste heat and expands at an elevated pressure and temperature to produce useful work [4]. Several types of fluid based power cycles have been proposed including Organic Rankine Cycle (ORC), Trilateral Flash Cycle, Kalina Cycle, and Goswami Cycle [8]. Among the TEG and power cycle methods, the Organic Rankine Cycle (ORC) is well established for waste heat recovery from low and medium grade heat sources because of its high thermal efficiency, less weight, smaller volume, simplicity and availability of the components [8, 9].

The ORC uses organic working fluid instead of water which can be often seen in the Rankine cycle. The organic fluid can have desirable properties such as a high molecular weight, high vapor pressure and low boiling point, and are capable of producing power from a few kW to 200kW with low and medium grade heat sources [10, 11]. Many factors including working fluid selection and operating condition can influence the performance of the ORC waste heat recovery system [12]. Glover *et al.* [13] studied the selection of working fluids and their boundaries and investigated the theoretical potential of work output and pressure-temperature limits of the selected fluids. Saleh *et al.* [14] presented the performance analysis of the ORC for geothermal application with regards to 31 pure organic fluids. Gao *et al.* [8] studied 18 different working fluids in an aim to find the best fluids to enhance the performance idicators, such as, power output, exergy efficiency, and lower investment. Most of the previous studies on the fluid selection were conducted using a thermodynamic based cycle, where isentropic and other mechanical losses are assumed to be constant.

*Corresponding author. Tel.: +44-(0)28-9097-4769, Fax.: +44-(0)28-9097-4148
E-mail address: b.nguyen@qub.ac.uk
† Recommended by Editor 000 000-please leave blank

In addition to the working fluid selection, the operating conditions of the ORC have a significant influence on the thermal efficiency and heat utilization of the WHR system. Two classified operating conditions of the ORC waste heat recovery system can be observed: subcritical and supercritical. The operating pressure of the subcritical ORC is below the critical pressure of the working fluid; while the supercritical ORC is run at a pressure higher than the critical pressure. Recent research on the ORC WHR under subcritical conditions has focused on parametric optimization [15-17], dynamic modelling and control [11, 18-20]. In subcritical conditions, Glover *et al.* [4] showed that the thermal efficiency of the ORC is low since the cycle is run at a lower pressure ratio. The supercritical ORC has been investigated with the aim to increase the cycle efficiency and presented in several reports [4, 8, 21]. The initial investigation outcome shows that the cycle efficiency of the ORC WHR system can be enhanced by 10% - 30% with the heat addition to working fluids at supercritical pressure, since specific work output and cycle efficiency is increased with the increase of pressure ratio [4, 8, 9]. In excess to the enhanced efficiency, the exergy degradation is low at the supercritical pressure which is an advantage to achieve high heat utilization of the WHR system [22]. Furthermore, other advantages including low compression work requirements to elevate the fluid temperature and pressure above the critical values, and a better thermal match between supercritical working fluids and heat sources have also been mentioned in [8, 14].

Although the supercritical ORC WHR has remarkable benefits, availability of components and safety of operation are the two major concerns for this area [23]. Simulation of the supercritical condition is, therefore, necessary before testing the real system. Research on the supercritical ORC WHR has focused, primarily, on the fluid selection [8, 13]; design and optimization [21, 22] only. To the author's knowledge, the supercritical ORC based waste heat recovery system using variable heat sources from an internal combustion engine has not been studied.

In this research, the ORC WHR system is investigated in supercritical conditions with variable heat sources from the real vehicle exhaust from the city and highway drive cycles. The aim of this simulation is to show the effects of operating parameters such as mass flow rate, temperature, evaporator pressure and condenser pressure on the performance of the waste heat recovery system.

The sections of the paper are presented as follows. Detailed ORC modelling techniques are described in section 2. Simulation results and comprehensive analysis are presented in section 3. Conclusions are drawn in section 4.

2. Modelling of the ORC WHR system

The ORC WHR system consists of four major components: pump, evaporator, expander and condenser as shown in Fig. 1. Liquid refrigerant is pumped to the evaporator where it is heated and vaporized by the engine's exhaust. This vaporized fluid is then expanded and produces mechanical energy in the shaft of the expander. A generator is normally coupled with the expander shaft to convert mechanical energy into electrical power. Exhaust product from the expander passes through the condenser where secondary cooling air removes extra heat and converts the exhaust back to a liquid.

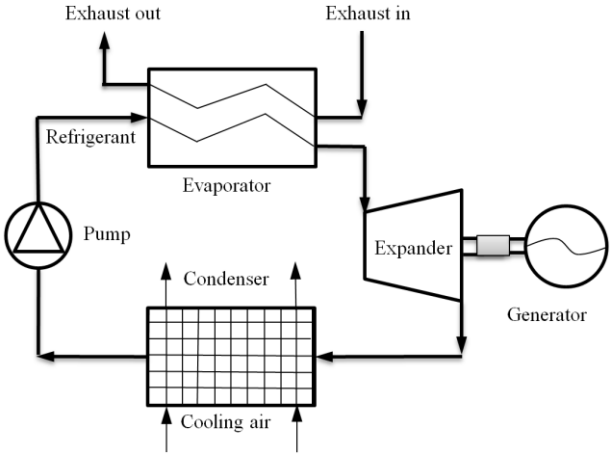

Fig. 1. ORC waste heat recovery circuit

This section describes a detailed model of the pump and evaporator including a thermodynamic model of the expander and condenser of the ORC WHR system.

2.1. Pump model

In this research, the volumetric diaphragm type Hydra-cell D/G-03-B pump with a maximum outlet and inlet pressure of 8300 kPa and 1700 kPa, respectively [24] is used in the simulation of the WHR system. The maximum speed of the pump can be up to 1750 RPM. The maximum delivery capacity of the pump at this speed is 4.2 litre/min. For volumetric diaphragm pumps, the mass flow rate is proportional to the speed of the pump [20, 25]. The relationship between pump speed and the mass flow rate of R134a at saturated liquid state is derived from the performance curve of the selected diaphragm pump provided by manufacturer as follows:

$$\dot{m}_p = 0.00002N_p + 0.0031 \tag{1}$$

where $\dot{m}_p$ is the mass flow rate of the pump in kg/s and N_p is the corresponding pump speed (RPM).

The enthalpy at the outlet of the pump H_{po} and work done W_p can be calculated as follows:

$$H_{po} = \frac{\bar{\upsilon}_p(P_{po} - P_{pi})}{\eta_p} + H_{pi} \tag{2}$$

$$W_p = \frac{\bar{\upsilon}_p(P_{po} - P_{pi})\dot{m}_p}{\eta_p} \tag{3}$$

where $\bar{\upsilon}_p$ is the specific volume (m^3/kg); H_{pi} is the enthalpy of the fluid (kJ/kg) at the inlet of the pump; η_p is the mechanical efficiency of the high pressure diaphragm pumps which is equal to 0.75 and assumed to be constant [2, 26]; P_{pi} and P_{po} are the pump inlet and outlet pressure, respectively.

The working fluid used in this simulation is R134a, which is widely used for commercial purposes, readily available and has a high auto-ignition temperature [13]. Since the critical pressure of the R134a refrigerant is 4060 kPa and temperature is 374 K, the supercritical pressure at the pump outlet in this simulation is set to 5500 kPa, which is well above the critical pressure. On the other hand, the inlet pressure of the pump is set to 770 kPa which is the minimum pressure at the nominal condenser temperature of 303 K [13].

2.2. Evaporator model

The evaporator is considered as the most important part of the ORC in this simulation since heat transfer at supercritical pressure takes place within this component. The selection of heat exchanger depends on the operating conditions, fluids and heat transfer requirements in the system. The common types of heat exchangers available in the market are finned tube, shell and tube, plate, etc. A counter flow plate heat exchanger is chosen as the evaporator in this research because of its compactness and outstanding heat recovery qualities [9]. The geometrical parameters of the evaporator are listed in Table 1.

Three modelling techniques are normally used for the evaporator: single segment lump method, three zone method and distributed or finite volume (FV) method [17]. The single segment technique treats the evaporator as a single-phase (i.e. liquid) heat exchanger. This method is appropriate when the specific heat of the fluid does not change with temperature. The zone modelling technique can be used where the evaporator has three distinct phases: liquid, liquid-vapor and superheat vapor zone. The heat transfer equations in each zone are solved by applying this method. In the finite volume technique, the evaporator is split into small segments and the thermo-physical properties are assumed to be constant at each segment since the temperature variation of the segment is low and is normally neglected.

When an evaporator is subjected to a supercritical pressure, the thermo-physical properties of the working fluid are strongly dependent on the temperature [22]. Furthermore, a distinct phase for the fluids does not exist at supercritical conditions. For these reasons, a single segment lump method with constant fluid properties or a zone-wise technique cannot be used to calculate the heat transfer in supercritical conditions. In order to take those property changes into account, the evaporator is divided into small segments along the flow direction as shown in Fig. 2, and the heat transfer equations for each segment are solved iteratively by the finite volume method [27].

The Finite Volume (FV) evaporator model uses refrigerant as the working fluid and the engine's exhaust as the secondary fluid. The model is built with the following fundamental assumptions:

a) There is no pressure loss in either the exhaust or refrigerant side of the heat exchanger.
b) Heat transfer from or to the surrounding environment is negligible.
c) Heat exchanger fouling is not included in the model.
d) Heat from the exhaust is completely transferred to the working fluid.

Table 1. Evaporator model parameter

Parameter	Quantity	Value
A	Heat transfer area of the evaporator	$3m^2$
$D_{h,g}$	Hydraulic diameter (gas side)	0.009m
$D_{h,l}$	Hydraulic diameter (liquid side)	0.004m
L	Length of each plate of the evaporator	0.3m
W	Width of each plate of the evaporator	0.119m
K	Thermal conductivity	15W/m K

The input and output parameters of the model are: mass flow rates ($\dot{m}_{exh}, \dot{m}_r$) and temperatures (T_{exh}, T_r) of the exhaust and refrigerant; and evaporator power (Q_r) and outlet temperature ($T_{r,o}$), respectively. Using this method, the outlet temperatures of the model are not known, but are initially estimated and an iteration process is carried out for each segment. The iteration starts from the 1^{st} segment and finishes at the N^{th} segment as shown in Fig. 2. For each segment or cell j in Fig. 2, the heat transfer from the exhaust to the wall Q_{exhj} and the wall to the refrigerant Q_{rj} can be calculated in Eq. (4) and (5) as follows:

$$Q_{exhj} = h_{exhj} A_{exhj} (T_{exh} - T_{wall})_j \quad (4)$$

$$Q_{rj} = h_{rj} A_{rj} (T_{wall} - T_r)_j \quad (5)$$

where h_{exhj} and h_{rj} refers to the convective heat transfer

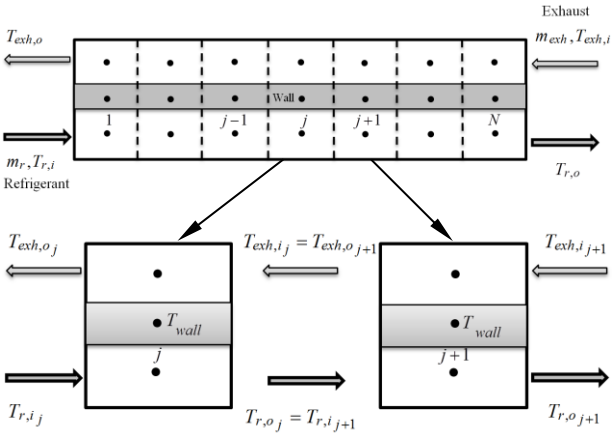

Fig. 2. Finite volume evaporator model

coefficients (kW/m^{2}K) of the exhaust and refrigerant, respectively, at cell j with the wall. The exhaust temperature of the cell j T_{exh_j} and refrigerant temperature T_{r_j} can be obtained as the average of the inlet and outlet temperature of the cell. The wall temperature T_{wall} can be evaluated from the average temperature of the exhaust and refrigerant of the cell. A_{exh_j} A_{exh_j} and A_{r_j} are the heat transfer surface areas of the cell in exhaust side and refrigerant side, respectively. The area of each cell A_j is obtained as follows:

$$A_j = \frac{A}{N} \tag{6}$$

where A is the total heat transfer area of the evaporator.

The amount of heat transferred due to the change in temperature of the exhaust Q_{exh_j} is calculated in Eq. (7) and the heat transferred due to the change in enthalpy of the refrigerant Q_{r_j} is calculated in Eq. (8) as follows:

$$Q_{exh_j} = \dot{m}_{exh_j} C_{p,exh_j} (T_{exh,i} - T_{exh,o})_j \tag{7}$$

$$Q_{r_j} = \dot{m}_{r_j} (H_{r,o} - H_{r,i})_j \tag{8}$$

where C_{p,exh_j} is the specific heat capacity of the exhaust (kJ/kg K); $T_{exh,i}$ and $T_{exh,o}$ are the exhaust temperature at the inlet and outlet of the evaporator respectively; $H_{r,i}$ and $H_{r,o}$ are the specific enthalpy (kJ/kg) of the refrigerant at the inlet and outlet of the evaporator, respectively.

The thermo-physical properties of the working fluid around the critical temperature are strongly variable at critical pressure [22]. For this reason, the Jackson correlation for supercritical fluids [28, 29] is used to calculate the Nusselt number Nu for the refrigerant in Equation (9). This neutralizes the variation effects around the pseudo-critical point.

$$Nu_r = 0.0183 \mathrm{Re}_b^{0.82} \mathrm{Pr}^{0.5} \left(\frac{\rho_{wall}}{\rho_b} \right)^{0.3} \left(\frac{\bar{c}_p}{c_{p_b}} \right)^n \tag{9}$$

$$\bar{c}_p = \frac{H_w - H_b}{T_w - T_b} \tag{10}$$

$n = 0.4$

for $T_b < T_{wall} < T_{pc}$ and $1.2T_{pc} < T_b < T_{wall}$

$$n = 0.4 + 0.2 \left(\frac{T_{wall}}{T_{pc}} - 1 \right) \tag{11}$$

for $T_b < T_{pc} < T_{wall}$

$$n = 0.4 + 0.2 \left(\frac{T_{wall}}{T_{pc}} - 1 \right) \left(1 - 5 \left(\frac{T_b}{T_{pc}} - 1 \right) \right)$$

for $T_{pc} < T_b < 1.2T_{pc}$ and $T_b < T_{wall}$

where T_b is the bulk temperature of the refrigerant, T_{pc} is the pseudo-critical temperature of the refrigerant; $\bar{c}_p$ is the average specific heat capacity of the medium; ρ_{wall} is the density of the working fluid at wall temperature and ρ_b is the density of the working fluid at bulk temperature; H_{wall} and H_b are the enthalpy of the working fluid at wall and bulk temperature, respectively. In this case, the bulk temperature is the same as the average refrigerant temperature of the cell.

For the exhaust, the Nusselt Number correlations proposed by Gnielinski are used. The proposed correlation takes wall roughness into account by calculating friction factor f_{exh} based on the Reynolds number Re as follows [9, 30]:

$$f_{exh} = (1.82 \log \mathrm{Re}_{exh} - 1.5)^{-2} \tag{12}$$

$$Nu_{exh} = \frac{(f_{exh}/8)(\mathrm{Re}_{exh} - 1000)\,\mathrm{Pr}_{exh}}{1.07 + 12.7(f_{exh}/8)^{0.5}(\mathrm{Pr}_{exh}^{2/3} - 1)} \tag{13}$$

for $\mathrm{Re}_{exh} > 10^4$ and $\mathrm{Re}_{exh} < (5 \times 10^6)$

$$Nu_{exh} = \frac{(f_{exh}/8)\,\mathrm{Re}_{exh}\,\mathrm{Pr}_{exh}}{1.07 + 12.7(f_{exh}/8)^{0.5}(\mathrm{Pr}_{exh}^{2/3} - 1)} \tag{14}$$

for $\mathrm{Re}_{exh} < 10^4$

where Re is the Reynolds number and Pr is the Prandtl number.

The convective heat transfer coefficients of the exhaust and refrigerant in Eq. (4-5) are calculated from the relationship among the Nusselt number, hydraulic diameter of the flow channel D_h and thermal conductivity of the fluid K as follows:

$$Nu = \frac{hD_h}{K} \tag{15}$$

Reynolds number Re in Eq. (9-14) is calculated using the relationship among the density ρ (kg/m^3), viscosity μ (Pa.s), velocity V (m/s) and hydraulic diameter of the fluid as follows:

$$\mathrm{Re} = \frac{\rho V D_h}{\mu} \tag{16}$$

Fig. 3 and Fig. 4 show the finite volume iteration process to calculate the outputs of the evaporator model. The steps of the iteration process are described below.

Step1: All inputs of the model, including flow rate of exhaust gas, temperatures of the fluids, pressure, refrigerant flow rate and geometry of the evaporator are defined at the beginning of the iteration process. Among these input variables, the refrigerant and exhaust variables are used as the inputs of the segment $j = 1$ and $j = N$ as shown in Figs. 2 and 3. The first segment is then initialized by assigning an initial inlet refrigerant temperature and assuming an initial exhaust outlet temperature as shown in Fig. 3.

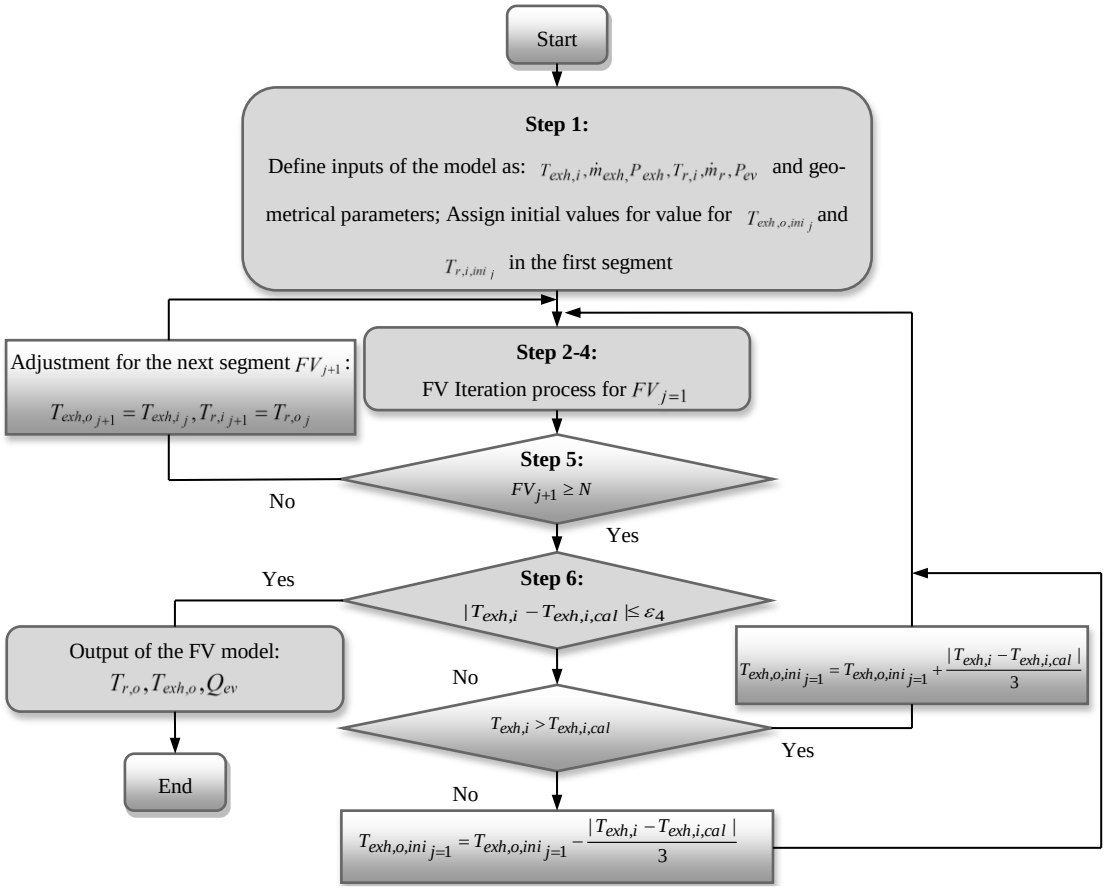

Fig. 3. Finite volume calculations for all segments of the evaporator

Step 2: Set the initial values for the inlet, outlet and wall temperatures of the segment $j = 1$ as shown in Fig. 4.

Step 3: When all inlet and outlet temperatures of the first segment are known, the convective heat transfer coefficients of the exhaust and refrigerant are calculated using Eq. (9-16). Once heat transfer coefficients of the fluids are obtained, the wall temperature of the evaporator is iteratively evaluated until the heat transfer rates in Eq. (4) and (5) are equal.

Step 4: The heat transfer rate of the fluids at step 3 is used to calculate the output variables of each segment by using the energy balance condition of the fluids. The calculated output variables are compared with the initially assumed values and the iteration process is repeated until the deviation is within the allowable limits of the convergence values as shown in Table 2. These values are a compromise chosen to reduce the computation time while achieving reasonable accuracy.

Step 5: At this stage, the outlet variables of the first segment are all known. The iteration process continues along the refrigerant flow direction, the output variables of the first segment are used as the input of the second segment as shown in Fig. 2. When the second segment is initialized with the input variables, the iteration process starts again to calculate the output variables and stops when the deviation is satisfied within the prescribed range. This process is repeated until the N^{th} segment, as shown in Fig. 3.

Step 6: At the end of the N^{th} segment, the calculated exhaust temperature at the inlet of the evaporator $T_{exh,i,cal}$ is obtained. The outlet temperature of the N^{th} segment is then compared with the real exhaust data. If the error between the calculated and real temperature is less than the deviation shown in Table 2, the iteration process stops. Otherwise, the iteration process is repeated as shown in Figs. 3-4.

Table 2. Convergence value for iteration loops

Convergence name	Convergence value
ε_1	0.3
ε_2	0.5
ε_3	0.5
ε_4	2

2.3. Expander model

The heat energy recovered at the evaporator is then expanded in the expander to generate mechanical rotational energy. A thermodynamic model based on the state enthalpy is used for the simulation of the expander in this research. The work output of the expander $W_{\exp}$ is calculated as follows:

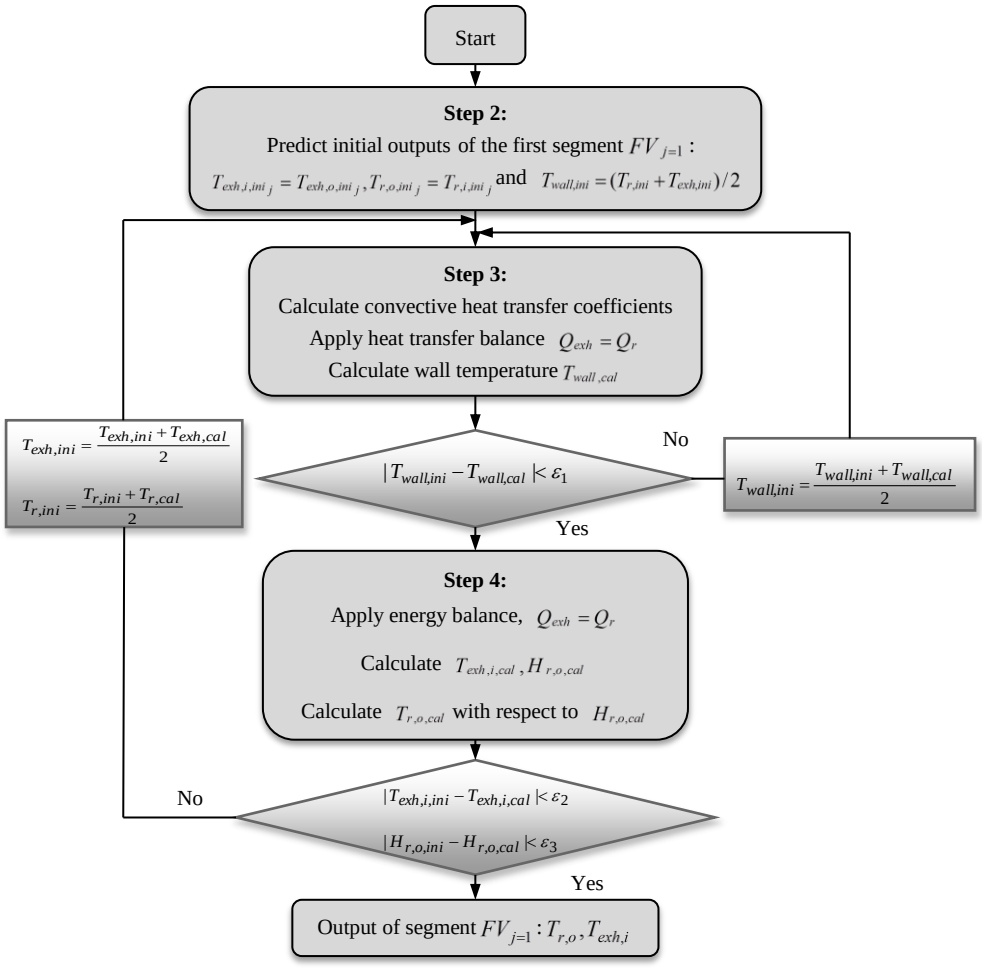

Fig. 4. Finite volume calculations for the first segment $FV_{j=1}$

$$W_{\exp} = \dot{m}_{\exp}\eta_{\exp}(H_{\exp,i} - H_{\exp,o}) \quad (17)$$

where $\dot{m}_{\exp}$ is the mass flow rate of refrigerant through the expander; $H_{\exp,i}$ is the enthalpy at the expander inlet and $H_{\exp,o}$ is the enthalpy at the expander outlet; $\eta_{\exp}$ is the mechanical efficiency of the expander, which is equal to 0.80 and assumed to be constant as shown in [2, 31].

2.4. Condenser model

The condenser is a heat transfer device that removes the heat from the vaporized refrigerant and returns it back to the liquid form. In the simulation, it is assumed that a sufficient amount of cooling air is supplied to the condenser so that the liquid-vapor refrigerant from the expander is cooled down to the initial inlet temperature of the pump.

A thermodynamic model of the condenser based on the state enthalpy represents the cooling power Q_{con} in the following equation.

$$Q_{con} = \dot{m}_{con}(H_{\exp,o} - H_{p,i}) \quad (18)$$

where $\dot{m}_{con}$ is the mass flow rate of refrigerant through the condenser which is the same as the mass flow rate of refrigerant at the pump. $H_{p,i}$ is the enthalpy at the inlet of the pump.

2.5. Overall model of the WHR system

The overall model of the cycle shown in Fig. 5 is built by interconnecting all subcomponents in the WHR system. The inputs and outputs of the adjacent components are as follows:

- The mass flow rates of the pump and through all other components are assumed to be equal,
  $\dot{m}_p = \dot{m}_{r,i} = \dot{m}_{r,o} = \dot{m}_{\exp} = \dot{m}_{\exp,o} = \dot{m}_{con}$
- Pressure at the pump outlet is equal to the pressure of the evaporator and at the expander inlet, such that $P_{p,o} = P_{ev,i} = P_{ev,o} = P_{\exp,i}$
- Pressure at the expander outlet and in the condenser is equal to the pressure at the pump inlet, such that $P_{\exp,o} = P_{con} = P_{p,i}$
- The enthalpy at the pump outlet and at the evaporator inlet are equal, $H_{p,o} = H_{r,i}$

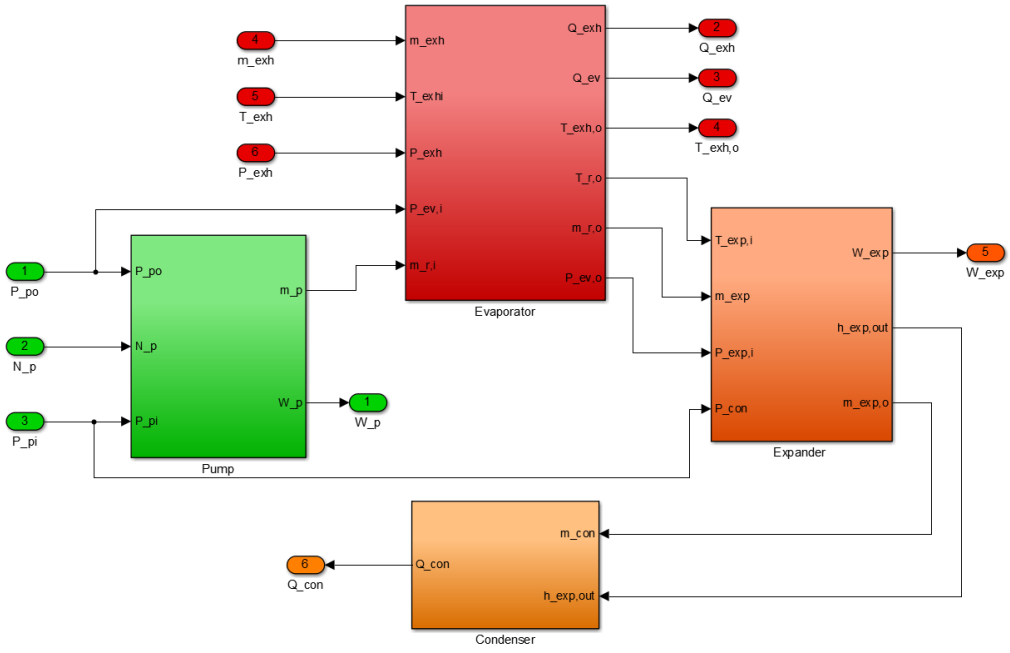

Fig. 5. Overall model of the ORC WHR system

- Enthalpy and specific volume of the refrigerant at the pump inlet is a function of inlet pressure, $H_{p,i}, \upsilon_p = f(P_{p,i})$ and the temperature of the refrigerant at the inlet of the evaporator is a function of the enthalpy and pressure at the pump outlet, $T_{r,i} = f(P_{p,o}, H_{p,o})$.

By interconnecting the individual inputs and outputs of each component, a set of overall model inputs-outputs can be defined and listed in Table 3.

2.6. Performance calculation

Three indicators can be used to investigate the performance of the ORC waste heat recovery system: cycle efficiency, heat recovery efficiency and overall system efficiency [18], as follows:

$$\eta_{cy} = \frac{W_{Net}}{Q_{ev}} = \frac{W_{\exp} - W_p}{Q_{ev}} \tag{19}$$

$$\eta_{hr} = \frac{Q_{ev}}{Q_{exh}} \tag{20}$$

$$\eta_{oa} = \eta_{cy} \times \eta_{hr} \tag{21}$$

where η_{cy} is the cycle efficiency, which is the ratio of net work output to the heat recovered at the evaporator, η_{hr} is the heat recovery efficiency which is defined as the amount of heat recovered from the given exhaust, and the overall system efficiency η_{oa} is the multiplication of the two other efficiencies and is defined as the ratio of the net work output to the available heat in the exhausts. Q_{ev} is the evaporator power which is obtained by using Eq. (8).

Table 3. Overall model parameters

Input parameters	Output parameters
$N_p, P_{p,i}, P_{p,o}, \dot{m}_{exh}, T_{exh,i}, P_{exh}$	$Q_{ev}, Q_{exh}, T_{exh,o}, W_p, W_{\exp}, Q_{con}$

The exhaust power $Q_{exh,av}$ in Eq. (22) is the total available heat of the engine's exhaust which is calculated by

$$Q_{exh,av} = \dot{m}_{exh}(H_{exh,i} - H_{exh,ref}) \tag{22}$$

where $H_{exh,i}$ and $H_{exh,ref}$ are the exhaust enthalpy at the inlet of the evaporator and at the reference temperature 298 K, respectively.

3. Simulation results

In this paper, exhaust data obtained from city and highway drive cycles of a hybrid car [4, 32] is used for the investigation of the waste heat recovery system in supercritical conditions. The mass flow rates and temperatures from the exhaust data for the drive cycles are shown in Figs. 6 and 7 respectively.

The organic fluid used in this simulation is R134a refrigerant. The R134a has the advantages of high auto-ignition temperature, readily available and less expensive.

All thermo-physical properties of the fluids are obtained from the NIST (National Institute of Standard and technology) database called REFPROP [33]. This database is used to calculate thermodynamic properties of the pure fluids and some predefined mixtures. The thermo-physical properties of the R134a can be provided within the temperature range from 169.85 K to 682 K in the REFPROP database.

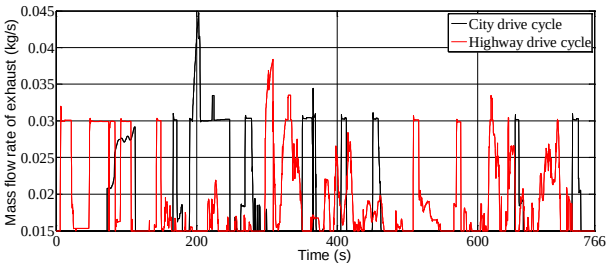

Fig. 6. Exhaust flow rates of the vehicle drive cycles

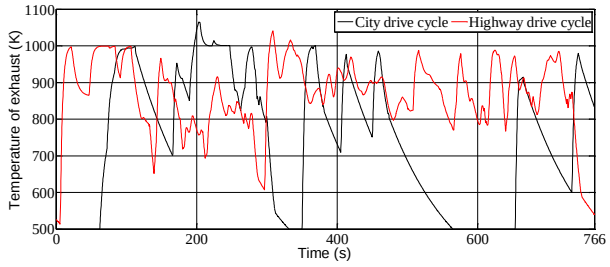

Fig. 7. Exhaust temperature of the vehicle drive cycles

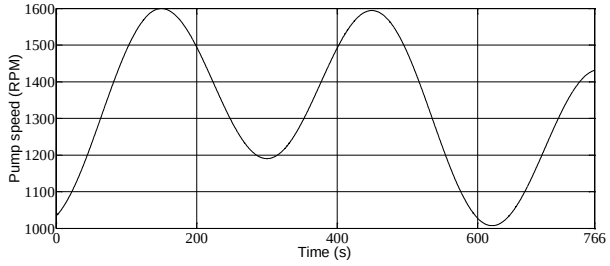

Fig. 8. Random pump speed profile for the simulation of entire drive cycles

The sampling time is set to 0.25s for the simulation and the mass flow rates are assumed to be constants during each step. The number of segments of the evaporator is set to 20, as it can ensure good agreement between iteration time and accuracy of the simulation.

Simulation of the waste heat recovery system in this research is presented with the entire operating range of the drive cycles and with selected points of the exhaust data. The following sections describe the simulation results in detail.

3.1. Investigation of entire drive cycles

To investigate the effect of operating parameters on the system outputs, a random pump speed profile ranging from around 1000 RPM to 1600 RPM, as shown in Fig. 8, is used in the simulation. The minimum speed is set to around 1000 RPM to ensure the mass flow rate of the R134a refrigerant not to drop to a level that allows its temperature to exceed the allowable limits in the REFPROP. The maximum limit is set to 1600 RPM which is below the highest speed of the selected pump as discussed in section 2. The simulation results of the entire drive cycles are presented in Figs. 9 -14.

The fluctuation of evaporator outlet temperature is shown in Fig. 9, in which a minimum and maximum temperature of 361 K and 533 K for highway drive cycle and 356 K and 527 K for city drive cycle, respectively, are observed. The maximum temperature obtained in the simulation is lower than the upper limit of the evaporator temperature of R134a, which is bounded by its auto ignition temperature of 1023 K.

The fluctuation of heat transfer rates in the evaporator is shown in Fig. 10. It can be seen from Figs. 6-8 and 10 that a maximum of 12.8 kW of heat from the city drive cycle can be recovered at the exhaust flow of 0.0448 kg/s and 1065 K with the pump speed of 1483 RPM. Similarly, the maximum heat transfer rate obtained from the simulation of highway drive cycle is 11.4 kW with respect to 0.03 kg/s, 967 K and 1600 RPM.

The exhaust heat from the vehicle engine has the potential to produce 1-2 kW of energy in the expander when using the ORC WHR system in subcritical conditions [34]. Fig. 11 shows the potential expander power output of the system with respect to different drive cycles. The simulation results in Fig. 11 show that a maximum of 1.9 kW (gross) energy can be obtained in the expander when the drive cycles are simulated

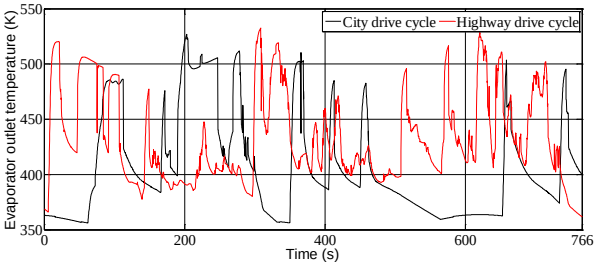

Fig. 9. Evaporator outlet temperature over entire drive cycles

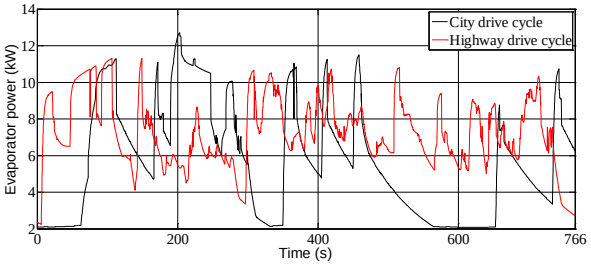

Fig. 10. Heat transfer rates over entire drive cycles

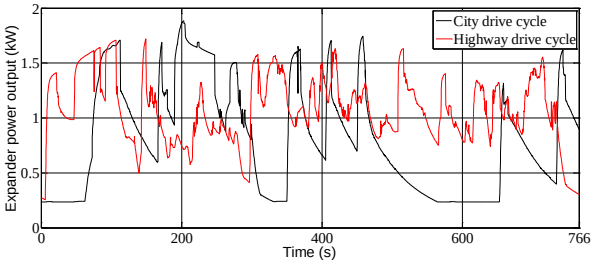

Fig. 11. Expander power output over entire drive cycles

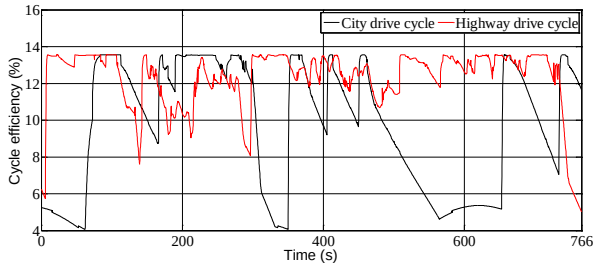

Fig. 12. Variation of cycle efficiency of the ORC WHR over entire drive cycles

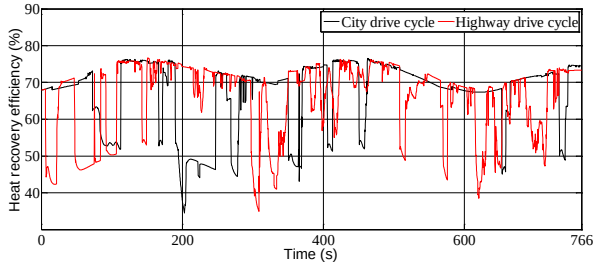

Fig. 13. Variation of heat recovery efficiency of the WHR over entire drive cycles

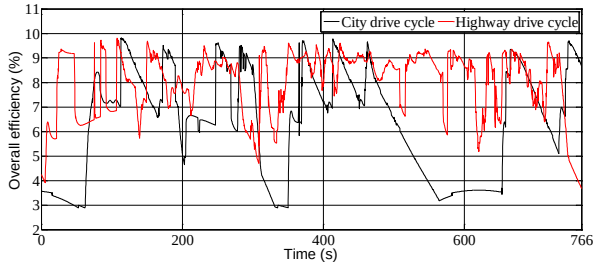

Fig. 14. Variation of overall system efficiency of the ORC WHR over entire drive cycles

at the supercritical pressure of 5500 kPa and with an expansion ratio of 7.14 (higher pressure 5500 kPa and lower pressure 770 kPa). Since the simulation is carried out with random mass flow rates of refrigerant, a higher power output could be achieved with an optimal control system. Although the power output for both drive cycles are in a similar range, the highway cycle is more favorable for expander operation because the variation of the exhaust mass flow rate and temperature drops are less than for those in the city drive cycle as shown in Figs. 6-7.

Figure 12 shows the ORC cycle efficiency for both entire drive cycles. With various combinations of model input profiles, the cycle efficiency for the simulation of drive cycles varies from 4.08% to 13.56%. Since the simulation was carried out with the random flow rate of the refrigerant and the model outputs were not optimized, the efficiencies are varied according to the combination of the input variables. Nevertheless, the heat recovery efficiency of the simulated model varies from 34% to 76% for the city drive cycle and from 35% to 77% for the highway drive cycle, as shown in Fig. 13. The percentage of heat recovered from the exhaust and converted into useful power in the expander is represented by an overall system efficiency which is shown in Fig. 14. The overall efficiency range obtained in the simulation is up to 9.80% for the both drive cycles.

3.2. Investigation of specific operating point

To simulate the effect of the variable mass flow rate of refrigerant on the performance of the WHR at constant heat flows, a specific operating point based on the average exhaust temperature and flow rate of the drive cycle data is selected. The exhaust mass flow rate and temperature of the selected operating point are $\dot{m}_{exh} = 0.025\,\text{kg/s}$ and $T_{exh} = 824\,\text{K}$ respectively. The pump speed, which generates the variable mass flow rate of the refrigerant, is increased gradually from 400 RPM to 1750 RPM. At this speed range, the evaporator outlet temperature stays within the REFPROP limits in this simulation. Results from the simulation of specific operating point are shown in Figs. 15-27.

The relationship between the mass flow rate of the refrigerant and evaporator outlet temperature at the constant heat flow

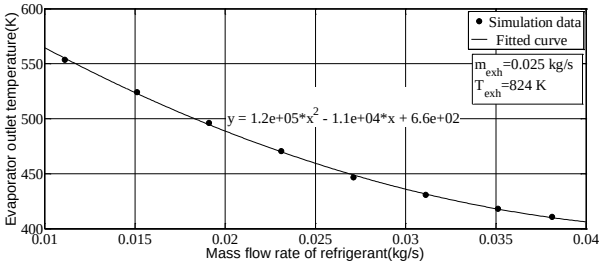

Fig. 15. Variation of evaporator outlet temperature with respect to mass flow rate of refrigerant

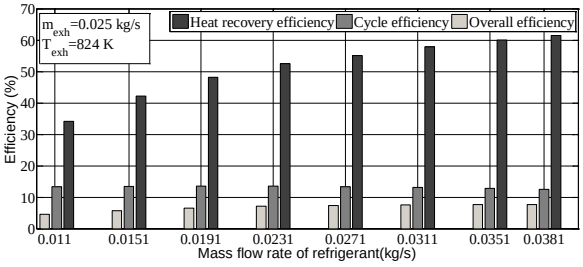

Fig. 16. Variation of ORC WHR efficiencies with respect to mass flow rate of refrigerant

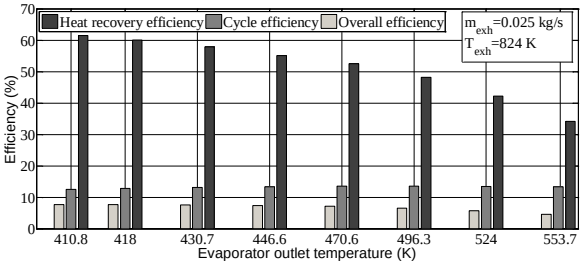

Fig. 17. Variation of ORC WHR efficiencies with respect to evaporator outlet temperature

is shown in Fig. 15. For the given exhaust flow and temperature, the evaporator outlet temperature decreases with the increase of the refrigerant flow rate by following the polynomial equation.

$$T_{ev} = 120000 m_r^{\,2} - 11000 \mathrm{m_r} + 660 \quad (23)$$

This decrease is caused by a higher mass flow rate of refrigerant flow against a constant heat input to the evaporator, which means that the evaporator absorbs more heat and therefore the outlet temperature of the refrigerant is decreased.

Figure 16 shows the variation of efficiencies at different refrigerant flow rates. This figure demonstrates that when the mass flow rate increases, the cycle efficiency also increases up to a maximum value, after which it declines. This is because when the mass flow rate of refrigerant is too high, the temperature at the evaporator outlet is reduced to a point where the evaporator power is much higher, but the specific enthalpy difference and work output is lower according to Eq. (17). This lower work output and higher evaporator power yields lower cycle efficiency according to Eq. (19). It can also be seen from this figure that the heat recovery efficiency can be improved by increasing the refrigerant mass flow. But this improvement is achieved by compromising the lower cycle efficiency as shown in Fig. 16. The overall system efficiency calculated in Eq. (21) is also shown in this figure for different mass flow rates. A maximum of 7.7% overall efficiency is achieved at a mass flow rate of 0.0351 kg/s of refrigerant.

The effect of the evaporator temperature on the various efficiencies including heat recovery efficiency is shown in Fig. 17. A contrasting effect is observed with the mass flow rate, where the increase in evaporator temperature causes a decrease in the heat recovery efficiency because the expander exhaust is cooled down at the higher temperature. In the simulation, the ORC WHR can obtain the highest efficiency at the temperature of 418K with a constant heat flow. The figure also shows that the highest overall efficiency of 7.7% and a corresponding cycle and heat recovery efficiency of 12.8% and 60.1%, respectively, can be achieved at this optimum temperature. The simulation results from Figs. 15-17 also show that the highest efficiency of the ORC can be obtained with the optimum temperature but not with the higher temperature.

3.2.1. Effect of evaporator pressure

An investigation of the effect of supercritical pressure and mass flow rate of refrigerant on various performance indicators of the WHR process is presented in this section. The three supercritical pressures selected for the simulation are as follows: 5500 kPa, 6500 kPa and 7000 kPa. These values are higher than the critical pressure of the R134a. However, the condenser pressure of 770 kPa is kept the same as before. The variation of operating parameters and performance indicators at different pressures and mass flow rates are shown in Figs. 18-22.

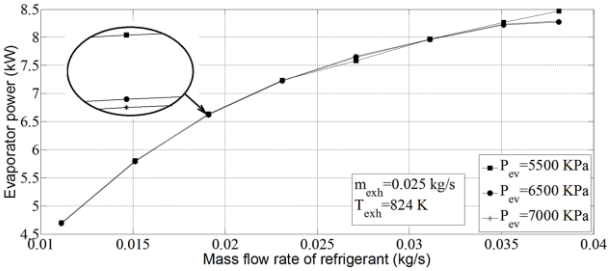

Fig. 18. Influence of supercritical pressure on evaporator power at different refrigerant flow rates

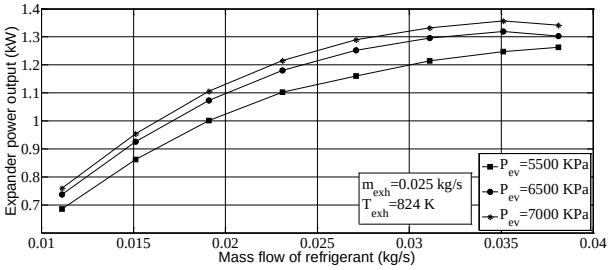

Fig. 19. Influence of supercritical pressure on expander power at different refrigerant flow rates

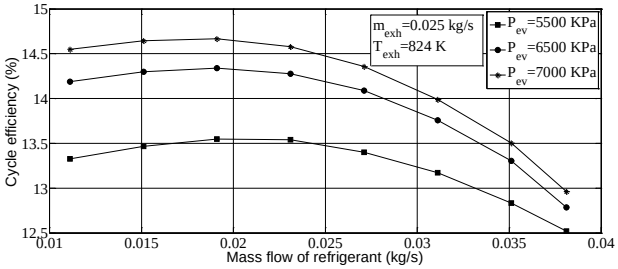

Fig. 20. Influence of supercritical pressure on cycle efficiency at different refrigerant flow rates

The results from the investigation of the effect of supercritical pressure on the evaporator power are shown in Fig. 18. The result shows that an increase in the evaporator pressure causes a decrease in the heat recovery in the evaporator. Fig. 21 provides evidence that for a given constant heat exchange area, the heat recovery efficiency of the WHR process decreases with the increase of the evaporating pressure. However, high pressure in the evaporator leads to a higher pressure ratio, which gives a higher work output in the expander as shown in Fig. 19.

The influence of supercritical pressure on the cycle efficiency of the ORC is shown in Fig. 20. It is clearly shown that the cycle efficiency of the ORC increases with the increase of the supercritical fluid pressure. The maximum cycle efficiency among the three cases is 14.67%, which is obtained at the supercritical pressure of 7000 kPa. The effect of the three different evaporating pressures on the overall system efficiency is shown in Fig. 22. The maximum overall efficiencies of 7.7%, 7.95 % and 8.1% can be obtained when the system operates at the supercritical pressure of 5500 kPa, 6500 kPa and

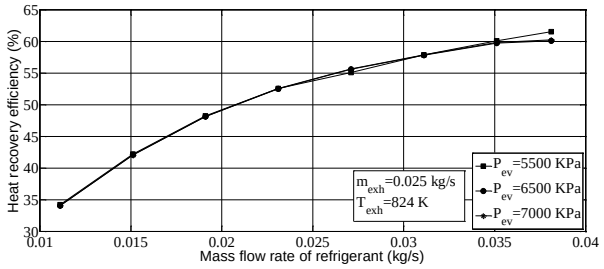

Fig. 21. Influence of supercritical pressure on heat recovery efficiency at different refrigerant flow rates

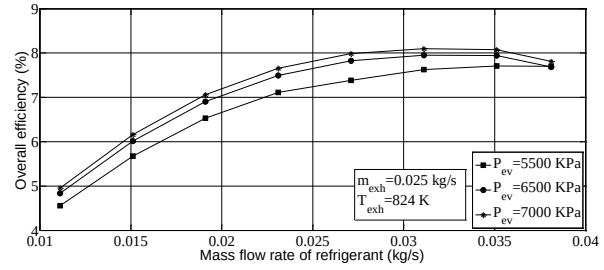

Fig. 22. Influence of supercritical pressure on overall system efficiency at different refrigerant flow rates

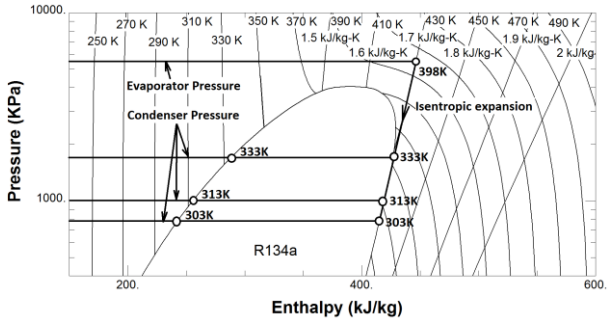

Fig. 23. Pressure enthalpy diagram of R134a

7000 kPa respectively. It can be seen from the simulation results that a 27% higher pressure in the system could enhance the cycle efficiency by 8.2% and the overall system efficiency by 5.2%.

3.2.2. Effect of condenser pressure

There are two methods to increase the specific work output of the expander in the ORC. One is to operate the system at a high evaporating pressure and the other is to maintain the condenser pressure as low as possible. Both methods increase the work output due to the increasing of the pressure ratio of the system. In order to investigate the effect of the condenser pressure on the performance parameters of the ORC WHR system, three different condenser pressures: 770 kPa, 1000 kPa and 1680 kPa were chosen with respect to the nominal condenser temperatures of 303 K, 313 K and 333 K as shown in Fig. 23. An isentropic expansion from the minimum evaporator temperature of 398 K and a supercritical pressure of 5500 kPa to the selected condenser temperatures and pressures can ensure that the expansion process is not in the wet region as shown in the pressure-enthalpy diagram of R134a in Fig. 23. However, the results shown in Figs. 24-27 are from the simulation of the WHR process at three different condenser pressures when the evaporator pressure is maintained at 5500 kPa.

The power output of the WHR system is calculated by an isentropic expansion, which is the difference between enthalpies at the inlet and at the outlet of the expander as discussed in section 2. When the condenser pressure increases,

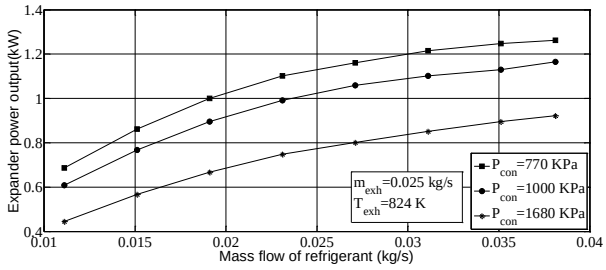

Fig. 24. Influence of condenser pressure on expander power at different refrigerant flow rates

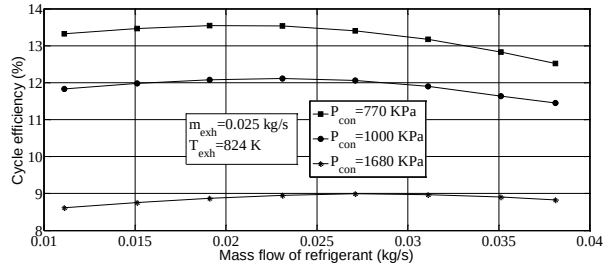

Fig. 25. Influence of condenser pressure on cycle efficiency at different refrigerant flow rates

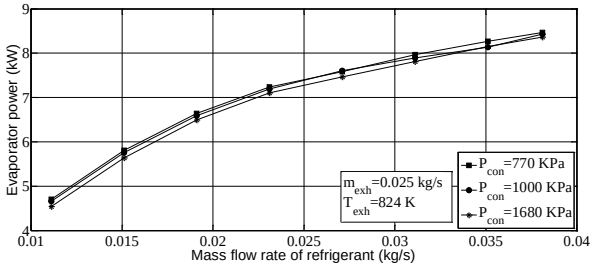

Fig. 26. Influence of condenser pressure on evaporator power at different refrigerant flow rates

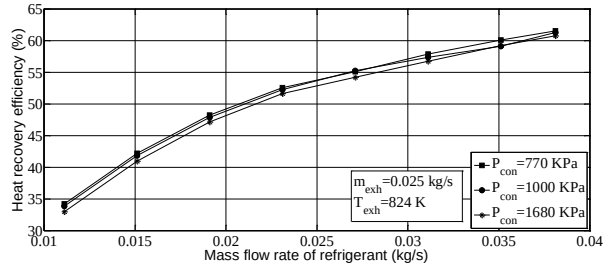

Fig. 27. Influence of condenser pressure on heat recovery efficiency at different refrigerant flow rates

the temperature also increases. As a result, the expansion ratio decreases and the expander exhaust products are cooled down at a higher temperature as shown in Fig. 23. This reduces the work output and consequently, the thermal efficiency of the system as noticed in Figs. 24 and 25. The result also shows that the condenser with 118% more pressure could reduce the thermal efficiency of the ORC system by 50.7%.

However, the investigation of the effect of condenser pressure on the evaporator power and heat recovery efficiency shows that the WHR system at 770 kPa condenser pressure can recover about 6% more heat than when the condenser operates at 1680 kPa (Figs. 26-27). This is as expected since the condenser pressure is assumed to be the same as the pump inlet pressure, and a low refrigerant temperature at the inlet of the evaporator is possible when the latter pressure is low as well. This low temperature is able to extract the maximum amount of heat from the exhaust, and therefore a higher heat recovery in the evaporator and higher efficiency of the system can be obtained.

4. Conclusions

The simulation of the ORC based WHR system with the variable exhaust data from real vehicle drive cycles (highway and city) is presented in this paper. The effects of the processing parameters including evaporator and condenser pressure, mass flow rate of refrigerant, and evaporator temperature on the performance parameters of the WHR process were investigated.

The developed model is suitable to depict the effect of mass flow rate of the refrigerant on the evaporator outlet temperature, which is the critical parameter for the control of the WHR system in real time. The investigation of the ORC based WHR model within the entire drive cycle in this paper can provide an overall mapping and characterization of operating ranges of the waste heat recovery system. The simulation results show that the cycle efficiency is not improved by increasing the evaporator temperature only. An optimum control of the evaporator outlet temperature of the system can effectively utilize the heat and deliver maximum efficiency. Furthermore, in order to maximize the heat usage, the evaporator pressure should be kept as high as possible while the condenser pressure should be kept as low as possible.

As the WHR process in automobile applications is associated with transient heat sources in the hot side and slow changes in the cold side of the evaporator; it is necessary to incorporate the thermal inertia into the system modelling. This will be the focus of future research in this area.

Acknowledgment

This work supported by the Queen's special research scholarship, School of Mechanical and Aerospace Engineering, Queen's University Belfast, UK. Sponsored body is gratefully acknowledged.

Nomenclature

A	:	Heat transfer area, m^2
C_p	:	Specific heat capacity, kJ/kg.K
D	:	Hydraulic diameter, m
f	:	Friction factor
H	:	Specific enthalpy, kJ/kg
h	:	Heat transfer coefficient, kW/m^2K
L	:	Plate length, m
$\dot{m}$	:	Mass flow rate, kg/s
N_p	:	Rotational speed of the pump, RPM
N	:	Number of segments
Nu	:	Nusselt number
P	:	Pressure, kPa
Pr	:	Prandtl number
Q	:	Heat power, kW
Re	:	Reynolds number
T	:	Temperature, K
V	:	Volume, m^3 or velocity, m/s
W	:	Power output, kW or plate width, m
ρ	:	Density, kg/m^3
υ	:	Specific volume,m^3/kg
ε	:	Convergence name
η	:	Efficiency
μ	:	Dynamic viscosity, Pa.s

Subscripts

av	:	Available
b	:	Bulk
cal	:	Calculated
con	:	Condenser
cy	:	Cycle
ev	:	Evaporator
exp	:	Expander
exh	:	Exhaust
hr	:	Heat recovery
i	:	Inlet
j	:	Segments notation
l	:	Liquid
o	:	Outlet
oa	:	Overall
p	:	Pump
pc	:	Pseudo-critical
r	:	Refrigerant
ref	:	Reference
wall	:	Evaporator wall

References

[1] Y. Glavatskaya, P. Podevin, V. Lemort, O. Shonda and G. Descombes, Reciprocating Expander for an Exhaust Heat Recovery Rankine Cycle for a Passenger Car Application, *Energies*, 5 (6) (2012) 1751-1765.

[2] A. Boretti, Recovery of exhaust and coolant heat with R245fa organic Rankine cycles in a hybrid passenger car with a naturally aspirated gasoline engine, *Applied Thermal Engineering* , 36 (2012) 73-77.

[3] H. Zhang, E. Wang and B. Fan, Heat transfer analysis of a finned-tube evaporator for engine exhaust heat recovery, *Energy Conversion and Management* , 65 (2013) 438-447.

[4] S. Glover, R. Douglas, L. Glover and G. McCullough, Preliminary analysis of organic Rankine cycles to improve vehicle efficiency, *Proceedings of the Institution of Mechanical Engineers, Part D: Journal of Automobile Engineering*, 228 (10) (2014) 1142-1153.

[5] M. Imran, B.-S. P. Park, H.-J. Kim, D.-H. Lee and M. Usman, Economic assessment of greenhouse gas reduction through low-grade waste heat recovery using organic Rankine cycle (ORC), *Journal of Mechanical Science and Technology* , 29 (2) (2015) 835-843.

[6] D. Rowe and G. Min, Evaluation of thermoelectric modules for power generation, *Journal of Power Sources* , 73 (2) (1998) 193-198.

[7] J. Liebl, S. Neugebauer, A. Eder, M. Linde, B. Mazar and W. Stütz, The thermoelectric generator from BMW is making use of waste heat, *MTZ Worldwide*, 70 (4) (2009) 4-11.

[8] H. Gao, C. Liu, C. He, X. Xu, S. Wu and Y. Li, Performance Analysis and Working Fluid Selection of a Supercritical Organic Rankine Cycle for Low Grade Waste Heat Recovery, *Energies*, 5(9) (2012) 3233-3247.

[9] G. Shu, G. Yu, H. Tian, H. Wei and X. Liang, A Multi-Approach Evaluation System (MA-ES) of Organic Rankine Cycles(ORC) used in waste heat utilization, *Applied Energy* , 132 (2014) 325-338.

[10] M. O. Bamgbopa and E. Uzgoren, Numerical analysis of an organic Rankine cycle under steady and variable heat input, *Applied Energy*, 107 (2013) 219-228.

[11] J. Zhang, Y. Zhou, Y. Li, G. Hou and F. Fang, Generalized predictive control applied in waste heat recovery power plants, *Applied Energy*, 102 (2013) 320-326.

[12] E. Wang, H. Zhang, B. Fan and Y. Wu, Optimized performances comparison of organic Rankine cycles for low grade waste heat recovery, *Journal of Mechanical Science and Technology* , 26 (8) (2012) 2301-2312.

[13] S. Glover, R. Douglas, L. Glover, G. McCullough and S. McKenna, Automotive Waste Heat Recovery: Working Fluid Selection and Related Boundary Conditions, *International Journal of Automotive Technology*, 16 (3) (2015) 399-409.

[14] B. Saleh, G. Koglbauer, M. Wendland and J. Fischer, Working fluids for low-temperature organic Rankine cycles, *Energy*, 32 (7) (2007) 1210-1221.

[15] H. Tian, G. Shu, H. Wei, X. Liang and L. Liu, Fluids and parameters optimization for the organic Rankine cycles (ORCs) used in exhaust heat recovery of Internal Combustion Engine (ICE), *Energy*, 47 (1) (2012) 125-136.

[16] Z. Q. Wang, N. J. Zhou, J. Guo and X. Y. Wang, Fluid selection and parametric optimization of organic Rankine cycle using low temperature waste heat, *Energy*, 40 (1) (2012) 107-115.

[17] J. Sun and W. Li, Operation optimization of an organic rankine cycle (ORC) heat recovery power plant, *Applied Thermal Engineering* , 31(11-12) (2011) 2032-2041.

[18] S. Quoilin, R. Aumann, A. Grill, A. Schuster, V. Lemort and H. Spliethoff, Dynamic modeling and optimal control strategy of waste heat recovery Organic Rankine Cycles, *Applied Energy*, 88 (6) (2011) 2183-2190.

[19] G. Hou, R. Sun, G. Hu and J. Zhang, Supervisory Predictive Control of Evaporator in Organic Rankine Cycle (ORC) System for Waste Heat Recovery, *Proc. of International Conference on Advanced Mechatronic Systems*, Zhengzhou, China (2011) 306-311.

[20] J. Zhang, W. Zhang, G. Hou and F. Fang, Dynamic modeling and multivariable control of organic Rankine cycles in waste heat utilizing processes, *Computers and Mathematics with Applications* , 64 (5) (2012) 908-921.

[21] A. Schuster, S. Karellas and R. Aumann, Efficiency optimization potential in supercritical Organic Rankine Cycles, *Energy* , 35 (2) (2010) 1033–1039.

[22] S. Karellasa, A. Schusterb and A.-D. Leontaritis, Influence of supercritical ORC parameters on plate heat exchanger design, *Applied Thermal Engineering*, 33-34 (1) (2012) 70-76.

[23] H. Chen, D. Y. Goswami and E. K. Stefanakos, A review of thermodynamic cycles and working fluids for the conversion of low-grade heat, *Renewable and Sustainable Energy Reviews*, 14 (9) (2010) 3059-3067.

[24] Installation and service manual: Hydra-Cell Industrial Pumps, *Wanner engineering, Inc.*, Minneapolis, USA (2015).http://www.hydra-cell.com/product/D03-hydra-cell-pump.html

[25] S. Declaye, S. Quoilin, L. Guillaume and V. Lemort, Experimental study on an open-drive scroll expander integrated into an ORC (organic rankine cycle) system with R245fa as working fluid, *Energy*, 55 (2013) 173-183.

[26] S. Glover, R. Douglas, M. De Rosa, X. Zhang and L. Glover, Simulation of a multiple heat source supercritical ORC (organic rankine cycle) for vehicle waste heat recovery. *Energy*, 93(2015) 1568-1580.

[27] J. Patiño, R. Llopis, D. Sánchez, C. Sanz-Kock, R. Cabello and E. Torrella, A comparative analysis of a CO2 evaporator model using experimental heat transfer correlations and a flow pattern map, *International Journal of Heat and Mass Transfer*, 71 (2014) 361–375.

[28] J. D. Jackson and W. B. Hall, Forced convection heat transfer to fluids at supercritical pressure, *Turbulent*

Forced Convection in Channels and Bundles, S. Kakac and D. B. Spalding, Eds. Hemisphere, New York, USA (1979) 563-611.

[29] J. D. Jackson and W. B. Hall, Influences of buoyancy on heat transfer to fluids flowing in vertical tubes under turbulent conditions, *Turbulent Forced Convection in Channels and Bundles*, S. Kakac and D. B. Spalding, Eds. Hemisphere, New York, USA (1979) 613-640.

[30] I. P. Kandylas and A. M. Stamatelos, Engine exhaust system design based on heat transfer computation. *Energy Conversion and Management*, 40 (10) (1999) 1057-1072.

[31] J. Zhang, Y. Zhou, R. Wang, J. Xu and F. Fang, Modeling and constrained multivariable predictive control for ORC (organic rankine cycle) based waste heat energy conversion systems. *Energy*, 66 (2014) 128-138.

[32] J. I. Chowdhury, B. K. Nguyen, D. Thornhill, R. Douglas, S. Glover, Modelling of organic Rankine cycle for waste heat recovery process in supercritical condition. *International Journal of Mechanical, Aerospace, Industrial, Mechatronic and Manufacturing Engineering*, 9(3), (2015) 453 - 458.

[33] E. W. Lemmon, M. L. Huber and M. O. McLinden, NIST Standard Reference Database 23: *Reference Fluid Thermodynamic and Transport Properties-REFPROP*, Version 9.0, National Institute of Standards and Technology, Gaithersburg, USA (2010).

[34] T. Horst Abbe, H.-S. Rottengruber, M. Seifert and J. Ringler, Dynamic heat exchanger model for performance prediction and control system design of automotive waste heat recovery systems, *Applied Energy*, 105 (2013) 293-303.